Effect of Fault Detection on The Resilience and Self-Healing in Islanded Micro-Grids

Reza Ebrahimi , Mohammad Hasan Moradi, Alireza Jahangiri* , Mohammad Abedini

Department of Electrical Engineering, Hamedan branch, Islamic Azad University, Hamedan, Iran.
ebrahimir094@gmail.com, mh_moradi@yahoo.com.uk, a.jahangiri@iauh.ac.ir, m.abedini@abru.ac.ir

Abstract

Fast protection and the existence of a resilient network play an important role in the stability of the power system. Today, with the expansion of the power grid and the increasing need for energy, the presence of highly resilient resources to prevent more frequent power outages is felt. The goal of this article is rapid detection of various types of faults, short circuits, and their compensation, leading to improved resilience and better operation of two islanded micro grids. The network under study is a 14-bus network selected according to IEEE standards. This network transforms into 2 micro grids in the event of a fault or incident. The micro grids are disconnected from the main network but remain interconnected with each other. This model is examined in three stages. The first stage is fault detection. The fault is identified and eliminated in the shortest possible time using the proposed algorithm based on the initial traveling wave currents caused by the fault using wavelet transform. The second stage deals with fault compensation using D-STATCOM. In the third stage, flexible operation is performed using responsive loads and CPP (critical peak pricing) prices based on game theory (cooperative game). Then resilience parameters and self-healing index are checked. Necessary loads of the total load are considered in assessing self-healing. Therefore, by using quick and timely fault detection, which leads to the use of voltage drop compensators, it can be concluded that the MOP index of consumers is also ensured. Additionally, considering the interconnection of micro grids, any micro grid that requires energy can be supplied by another micro grid.

Keywords: flexible operation, short-circuit fault detection, wavelet transform, micro grid, resilience, self-healing, Renewable Energy.
Article history: Received 2025/06/02, Revised 2025/07/25; Accepted 2025/08/19, Article Type: Research paper

https://doi.org/10.82234/IJSEE.2025.1210109

1. Introduction

The energy crisis is currently one of the newest issues in the world. The organization of global meetings and the development of various solutions to this crisis demonstrate the significance of the energy issue. There are concepts in the power system that do not have a long life in this system, all of which are related to better energy use and resolving the aforementioned problems. This category includes the concepts of microgrid, smart grid, energy hub concept, reliability, and flexibility. A multi-carrier energy network is a system made up of various energy carriers such as electricity, natural gas, and heat. In fact, a multi-carrier energy system can be thought of as a set of energy hubs connected by various networks. Energy is transmitted via networks and converted before being stored in energy hubs [2]. Custom Power introduces electronic power devices to improve power quality in distribution systems. FACTS devices operate to better control the power passing through the network and increase the load in the transmission system, up to the equipment's thermal range. Custom Power equipment, on the other hand, aims to improve the reliability and quality of power in distribution networks. Dynamic voltage recovery (DVR), static synchronous compensator or dynamic compensation of reactive power and voltage control (STATCOM), UPQC, which is a combination of D-FACTS and DVR, and DSSC, which is a combination of low-power modules, are all examples of Custom Power equipment. This equipment is based on the working principles of the VSC voltage source converter, and it corrects network disturbances by injecting voltage into the system.

A) Literature review and contribution

Previously, different energy networks, such as electricity and natural gas, were planned and implemented separately [1]. Although this may have an impact on the optimal performance of energy, independent methods were used to operate these energy carriers. However, the increased use of dispersed energy resources, as well as concern about their improper exploitation and coordination, led to an increase in incentives to create coordination in various energy networks [2]. Many studies have been conducted in recent years on the future perspective of energy based on the structure and limitations of the current management system. Following these studies, they discovered that for better resource management, different energy resources should be considered as an integrated system and that discrete energy carriers are not cost-effective; as a result, a new concept known as a "multi-carrier energy system" was proposed [3]. In contrast to these studies, the University of Zurich launched a project called "Vision of Future Energy Networks" in 2002. First, all existing energy structures were examined, and the desired structure was predicted for the next 50 years. With the simultaneous use of various energy resources in the form of the energy hub concept, a new window on optimal energy management was opened. As a new concept, the energy hub required a new structure and formulation, one that could operate multiple carriers in a coordinated platform. With the increased number of distribution network loads sensitive to voltage fluctuation (voltage swing) and the need for these loads to operate at a constant voltage, tools such as DVR and STATCOM are required. In recent decades, electronic equipment has emerged that are sensitive to power quality. Meanwhile, the VSC principle has been used to model and analyze such controllers for a wide range of performances using distribution static-synchronous compensator (D-STATCOM) and dynamic voltage recovery (DVR). Because of the high cost of energy storage and electronic power switches, as well as the result of these two costs, which is CUSTOM POWER devices, it is necessary to use a method that reduces the power and injection current when a fault occurs, resulting in a reduction in the nominal power and size of the switches. Installing these tools in a network where DG exists is one of these methods. Because of the variety of electrical and electronic equipment in industries and distribution system loads, as well as economic concerns, Custom Power tools must be used and tested. There have been numerous studies conducted on the impact of CUSTOM POWER devices such as DVR and STATCOM on improving the power quality of power distribution networks, some of which are listed in the "References" section. [4] describes the factors that cause voltage sag, which is one of the power quality issues, as well as the relationships between its calculation and correction techniques in distribution systems. This research focuses on the modeling and analysis of CUSTOM POWER controllers, a new generation of power electronics-based equipment designed to improve the reliability and quality of electric currents in low-voltage distribution networks. In contrast to the mathematical models embedded in the code using a high-level programming language, the modeling approach used in this research is graphical in nature. PSCAD/EMTDC's fully advanced graphics facilities, which are available in the industry standard power system package, have been used to perform all aspects of model execution and extensive simulation studies. For the three CUSTOM POWER controllers: Distribution Static Compensator (D-STATCOM), Dynamic Voltage Restore (DVR), and Solid-State Transfer Switch (SSTS), graphical models suitable for electromagnetic transient studies (EMT) are presented. Comprehensive results are provided to assess each device's performance as a potential CUSTOM POWER solution. The types of Custom Power subcategory equipment, as well as their functions and applications, are described in [6]. The modeling approach used in this study is also graphical in nature. The following Custom Power devices have MATLAB/Simulink-based models: Shunt Active Power Filter, Static Transfer Switch (STS), Dynamic Voltage Restorer (DVR), and Unified Power Quality Conditioner (UPQC). In [7-9], DVR is introduced and simulated as suitable equipment for protecting sensitive loads against distribution network disturbances, and its application to correct voltage sag is discussed, and the amount of voltage injected by the DVR to compensate for voltage sag is calculated based on the injected power. [10] investigates the performance of D-STATCOM and DVR for voltage control in distribution networks using a novel control strategy. Travelling wave (TW)-based protection techniques can help to achieve ultra-high-speed protection of transmission lines using the high-frequency transients generated after the fault occurrence. The sign, magnitude and time intervals between the arriving waves at the relaying point contain some information about the fault location from which the fault could be identified in just a few milliseconds after the fault occurrence [11].

Although many studies are done on the resilient problem of the micro grids and fault detection, the competition of the micro grids in island mode regarding the CPP (critical peak pricing) demand response program and Effect of fault detection on the resilient and self-healing in islanded micro grids is not addressed in the literature.

Based on the literature review, given the complexity of current power systems, islanded

operations, and the necessity of having a highly resilient network are crucial. To achieve a self-healing network, several factors are needed. One of these factors is rapid fault identification for quick network protection. Therefore, this article utilizes a new algorithm for rapid protection in a microgrid. The performance of the network under study and the proposed algorithm is as follows:

The network under study consists of a 14-bus system according to the IEEE standard, comprising PV (Photovoltaic), wind turbines, CHP, transformers, and generators. This 14-bus system is transformed into two microgrids. These two microgrids are isolated from the main grid and are only interconnected with each other (operating in islanded mode). The connection between these two microgrids allows them to sell their surplus power to each other using CPP. This process unfolds in three stages. In the first stage, the proposed algorithm functions to protect against internal and external faults within these two microgrids. The fault is detected in the shortest possible time. The algorithm's performance is based on the initial traveling wave currents caused by the fault, which are identified using wavelet transform. For faults occurring within each microgrid, the detected traveling wave currents in different phases are different, while for faults occurring in the interconnections between the two microgrids, they have similar waveforms. This characteristic is used to distinguish between internal and external faults. Hence, the protection algorithm can detect internal and external faults. In the second stage, compensation for voltage sag is provided using D-STATCOM. In the third stage, flexible operation is performed for hazardous loads. Flexible operation includes the use of renewable resources, demand side management and CPP pricing. Then the resilience parameters are evaluated to measure the amount of self-healing of the grid. In summary, the new aspects of this scheme are as follows. Figure 1 shows the graphical abstract.

- Rapid fault identification in the interconnection lines of two islanded microgrids using a wavelet method
- Fault compensation in an islanded distribution microgrid using D-STATCOM
- Operation of islanded microgrids using critical peak pricing (CPP)
- Evaluation of self-healing under critical conditions (short-circuit faults)

2. Model Evaluation

To assess the performance accuracy of the protection algorithm, a 14-bus IEEE standard power system model was designed using EMTDC/PSCAD software for simulating various faults in the network, as shown in Figure 2. Additionally, MATLAB software was used for programming purposes. The transmission system under study is depicted in Figure 2. The relay under investigation is installed on line number one connected to bus number five in microgrid 2. The communication lines between microgrid 1 and 2 span 160 kilometers between buses 4 and 5 with a nominal voltage of 230 KV. The power system network data for the 14-bus system is obtained from reference [11].

A) Error detection process

When an error occurs in the transmission line between two sub-networks at a non-zero voltage, the sudden change in the fault phase voltage generates traveling waves that can propagate along the transmission line in both directions. The magnitude of the voltage and current traveling waves depends on the fault resistance and the characteristic impedance of the transmission line, and are expressed as follows [11]:

$$V = -\frac{z_0}{z_0 + 2R_f} V_f \quad (1)$$

$$I = -\frac{1}{z_0 + 2R_f} V_f \quad (2)$$

Where V_f is the instantaneous voltage magnitude at the time of the fault, z_0 is the characteristic impedance of the transmission line, and Rf is the effective fault resistance. The traveling waves generated by the fault along the transmission line propagate until they reach a point of discontinuity, such as a compacted element or another transmission line with a different characteristic impedance. At a point of

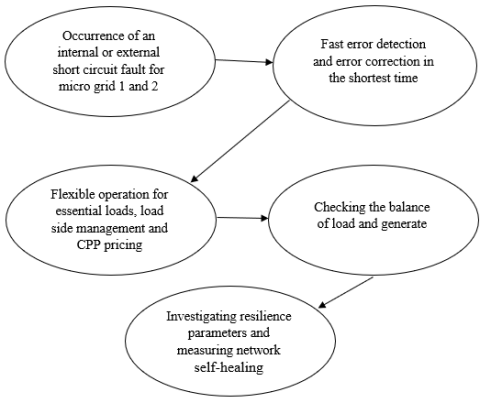

Fig. 1. Graphical abstract

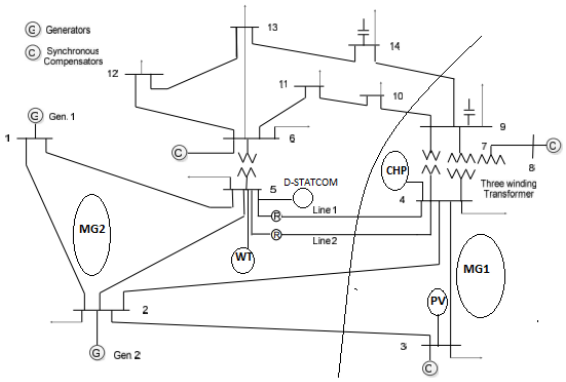

Fig. 2. IEEE standard 14 bus network investigated

discontinuity, a portion of the traveling waves passes forward and the rest is reflected backward. The reflection coefficients for the voltage and current traveling waves are given by the following equations:

$$K_V = \frac{z - z_0}{z + z_0} \quad (3)$$

$$K_i = -\frac{z - z_0}{z + z_0} \quad (4)$$

The z impedance is the impedance at the point of discontinuity where the propagated wave reaches along the transmission line. The propagation of traveling waves along transmission lines is nearly at the speed of light. Consequently, the propagated waves and reflections from the termination of the transmission line are simultaneously measured by the relay installed near the busbar. In other words, the signal measured by the relay is a combination of the propagated and reflected waves, presented as:

$$I_S = I + K_i I = \frac{2z_0}{z + z_0} I \quad (5)$$

Where I_S is the measured current signal by the relay. The reflected wave travels along the transmission line back to the point of fault, where it reflects again and returns to the relay path. The propagation of traveling waves in the transmission system continues until they are dissipated.

B) Wavelet Transform

As mentioned in the wavelet transform section, the wavelet transform is a method that decomposes the input signal into different frequency bands. This method expresses the results in both the time and frequency domains, making it a suitable mathematical tool for processing transient and unstable signals. The discrete wavelet transform decomposes the input signal using low-pass and high-pass filters. The outputs of the high-pass and low-pass filters are referred to as details and approximation coefficients, respectively. For example, a signal sampled at a frequency of 200 kHz is initially decomposed into frequency bands of 0-50 kHz and 50-100 kHz by the wavelet transform. In the next stage, the output of the low-pass filter, which is the frequency band of 0-50 kHz, is further decomposed into frequency bands of 0-25 kHz and 25-50 kHz, and this process continues. The decomposition stages are limited to n by the number of samples provided for the wavelet transform of the input signal. For example, for a signal with 2^n samples, a maximum of n decomposition stages can be achieved.

C) Protective Algorithm

The protective algorithm is based on six received signals consisting of the currents of the three-phase lines. Due to the frequency band of the traveling waves caused by errors in the transmission lines, the current signals are sampled at a speed of 200 kHz. The modal transformation is often used for analyzing three-phase systems. In this scheme, the Karenbauer modal transformation is used to separate the three-phase currents. The modal current components are calculated as follows [11]:

$$\begin{bmatrix} i_\alpha \\ i_\beta \\ i_0 \end{bmatrix} = \frac{1}{3}\begin{bmatrix} 1 & -1 & 0 \\ 1 & 0 & -1 \\ 1 & 1 & 1 \end{bmatrix}\begin{bmatrix} i_a \\ i_b \\ i_c \end{bmatrix} \quad (6)$$

The values of a, b, and c represent the phase currents, while α, β, and ω represent the modal values. The coefficients of the upper matrix are real numbers, so the modal values can be obtained by sampling the instantaneous values of the currents of all three phases. These features are very practical for analyzing transient signals. The Karenbauer transformation matrix is a regular matrix. Modal α represents the linear mode between phases a and b. Modal β represents the linear mode between phases a and c, and the modal components α and β cover various types of errors in each of the parallel lines. For covering errors between two circuits, the modal component γ is defined for the current signals as per equation 7-4.

$$i_\gamma = \frac{1}{3}(i_b - i_c) \quad (7)$$

The error features under the Karenbauer transformation for different types of errors can be calculated as follows:

The simplified diagram of single-phase to ground fault (phase A) is shown in Figure 3. Assuming that the ground resistance is zero and the boundary conditions are as follows:

$$u_a = 0 \ , \quad i_b = i_c = 0 \quad (8)$$

Therefore, the modal components are as follows:

$$\begin{bmatrix} i_\alpha \\ i_\beta \\ i_0 \end{bmatrix} = \frac{1}{3}\begin{bmatrix} i_a \\ i_a \\ i_a \end{bmatrix} \ , i_\gamma = 0 \quad (9)$$

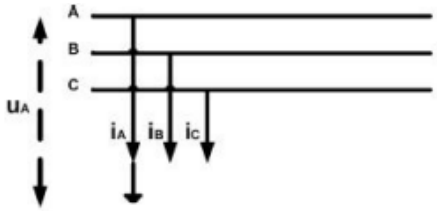

Fig. 3. Single-phase earth to ground

The simplified diagram of a two-phase fault (phase B and phase C) is shown in Figure 4 Assuming that the fault resistance is zero and the boundary conditions are as follows:

$$u_b = u_c \ , i_a = 0 \ , \qquad i_b = -i_c \tag{10}$$

$$\begin{bmatrix} i_\alpha \\ i_\beta \\ i_0 \end{bmatrix} = \frac{1}{3}\begin{bmatrix} -i_b \\ i_b \\ 0 \end{bmatrix} \ , \qquad i_\gamma = \frac{2}{3} i_b \tag{11}$$

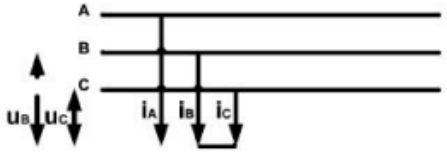

Fig. 4. Two phase faults

The simplified diagram of a three-phase to ground fault in Figure 5 is shown. Assuming that the fault resistance is zero and the boundary conditions are as follows:

$$u_a = u_b = u_c = 0 \ , \qquad i_a + i_b + i_c = 0 \tag{12}$$

$$\begin{bmatrix} i_\alpha \\ i_\beta \\ i_0 \end{bmatrix} = \frac{1}{3}\begin{bmatrix} i_a - i_b \\ i_a - i_c \\ 0 \end{bmatrix} \ , \qquad i_\gamma = \frac{1}{3}(i_b - i_c) \tag{13}$$

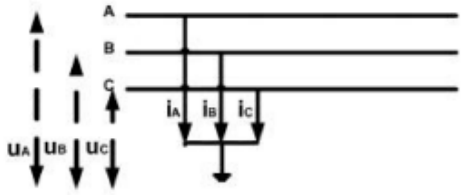

Fig. 5. Three phase to ground fault

According to Figure 6, when an internal fault occurs in each of the parallel circuits, especially at the moments when the first fault signals are detected, the fault circuit current includes the incident wave and its reflected wave from the relay location bus, while the healthy circuit current only includes a portion of the reflected wave [11]. Figure 5 illustrates the fault detection protection scheme. The maximum modal current signals in the frequency band of -50 to 100 kHz are used to determine the faulted circuit.

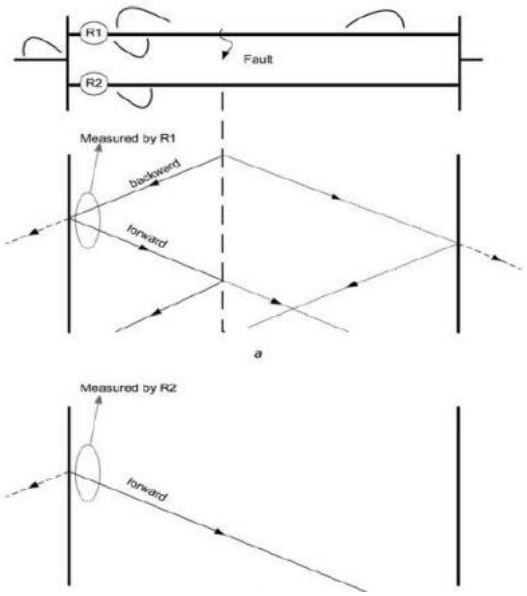

Fig. 6. Primary current waveforms of relay after the occurrence of an external fault (fault on communication lines between two sub-networks), a. Faulted lines b. Healthy lines

D) Mathematical modeling of EH's resources

For photovoltaic (PV) arrays and wind turbine (WT) units, the operation cost is zero and only the maintenance cost is considered as follows [6]:

$$C^{WT}(t) = P_e^{WT}(t) K_M^{WT} \tag{14}$$

$$C^{PV}(t) = P_e^{PV}(t) K_M^{PV} \tag{15}$$

The cost of power generation of CHP is modeled as (15). Also, the amount of power generation of CHP and its limitations are described as (16) and (17).

$$C^{CHP}(t) = P_l^{CHP}(t) K_o^{CHP} \qquad \forall l \in (e,h) \tag{16}$$

$$P_l^{CHP}(t) = P_g(t) \eta_l^{CHP} v^{CHP}(t) \quad \forall l \in (e,h) \tag{17}$$

$$P_{-l}^{CHP}(t) \le P_l^{CHP}(t) \le \bar{P}_l^{CHP}(t) \quad \forall l \in (e,h) \tag{18}$$

The technical constraints of the electrical and heat energy storage units are modeled as (18)-(20).

$$M_e(t) = S_e(t) E_e(t) \tag{19}$$

$$1 \le ES(t) \le ES^{max} \tag{20}$$

$$P_{-l}^{CHP}(t) \le P_l^{CHP}(t) \le \bar{P}_l^{CHP}(t) \quad \forall l \in (e,h) \tag{21}$$

$$E_{min}^{PHEVs} \le E^{PHEVs}(\omega, t) \le E_{max}^{PHEVs} \tag{22}$$

E) Mathematical model of resilience

$$OF = Max \sum_{\omega=1}^{\omega} \rho(\omega) RI(\omega) \tag{23}$$

$$\sum_{l=1}^{L} x_l C_l^H + \sum_{mg=1}^{3} x_{mg} C^{PHEVs} cap_{mg}^{PHEVs} \le B \tag{24}$$

$$RI = R_{mg1} + R_{mg2} + R_{mg3} \tag{25}$$

$$R_{mg} = SRI_1 + SRI_2 + SRI_3 \tag{26}$$

Figure 7. Basic social welfare is show. The value of each R is calculated based on the figure as follows:

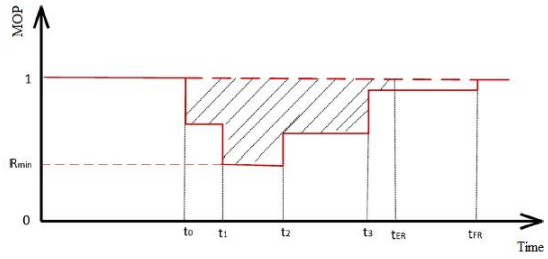

Fig. 7. Basic social welfare [7].

$$SRI_1 = R_{min} \qquad 0 \le SRI_1 \le 1 \tag{27}$$

$$SRI_2 = \frac{\int_{t_0}^{t_{ER}} MOP\ (t)dt}{t_0 * t_{ER}} \qquad 0 \le SRI_2 \le 1 \tag{28}$$

$$SRI_3 = \frac{t_{min}}{t_{FR}} \qquad 0 \le SRI_3 \le 1 \tag{29}$$

The second objective function, which is to reduce the rearrangement time, is written as follows:

$$OF_2 = Max \quad MOP \tag{30}$$

F) Load Distribution Equations:

Reactive power modeling is omitted because it can be provided locally.

$$P_{nm}(t) = \frac{V_n . V_m}{x_{nm}}\ sin\big(\delta_n(t) - \delta_m(t)\big) \tag{31}$$

$$P_{nm}(t) = B(t).sin\big(\delta_n(t) - \delta_m(t)\big) \tag{32}$$

$$P_e^{mg}(t) = \sum_{1}^{m} B_{nm}\ sin\big(\delta_n(t) - \delta_m(t)\big) \tag{33}$$

$$-line_{e,nm} < B_{nm}.\big(\delta_n(t) - \delta_m(t)\big) < line_{e,nm} \tag{34}$$

The electrical and heat energy balance for each micro grid is modeled as (35) respectively.

$$\begin{aligned} L_e^{MG}(t) + d_e(t) = {} & P_g(t)v^{CHP}(t)\eta_e^{CHP} \\ & + P_e^{DG}(t)\eta_e^{DG} + P_e^{WT}(t)\eta_e^{WT} \\ & + P_e^{PV}(t)\eta_e^{PV} - M_e(t) \end{aligned} \tag{35}$$

In this study, the operation of the power distribution network is modeled as a cooperative game, where players (micro grids) must cooperate while also competing with each other in order to prevent network failure. a micro grid may decide to earn less profit or even operate at a loss during certain hours and sell the output to another micro grid. However, this approach results in maximum satisfaction of the loads, which is equivalent to the Nash equilibrium of the problem we have:

$$G' = \left\langle I, K_i\big|_{i=1,2,3,\ldots,n_i}, Q_i\big|_{i=1,2,3,\ldots,n_i} \right\rangle \tag{36}$$

Here, I denote the players (microgrids), K_i is the strategy adopted by each player, and Q_i is the best performance of each player.

Nash equilibrium is obtained using the following equation:

$$Q_i\ (K_i^*, K_{-i}^*) \ge Q_i\ (K_i\ , K_{-i}) \tag{37}$$

G) Performance Review and Comparison of Wavelet Protection with Other Protections

The distance relay compares voltage and current, operating based on a criterion of the ratio between these two quantities. The methods for determining this ratio are related to the structure and function of the distance relay. Depending on the manufacturers' opinions, distance relays may vary. The basis of comparison between voltage and current in distance relays can be likened to a lever, as shown in Figure 8. In this case, the net torque controls the balance axis and can lead to issuing a command or the distance relay not working. The more realistic equivalent of the mentioned state can be checked by considering the power network of Figure 9. In this figure, the distance relay is placed at the post G and the lower transmission line is considered. The upper line has the same impedance as the lower line. Protection by relay A is expected to trip for phase faults in a fraction of the line length between G and H indicated by h_s. h_s is called distance relay percentage fraction. The impedance distance relay characteristic is shown in figure 10.

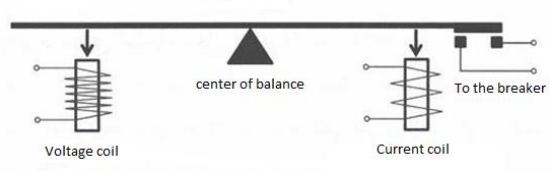

Fig. 8. Mechanical simulation of distance relay operation basis

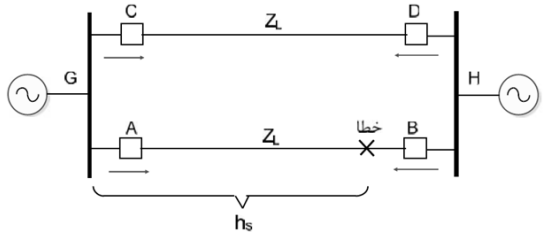

Fig. 9. Distance protection between G and H lines

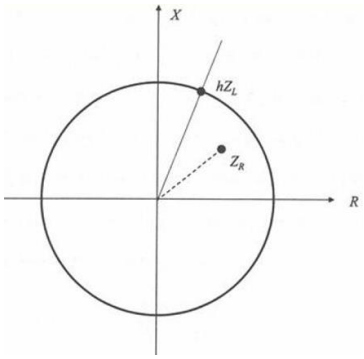

Fig. 10. Impedance distance relay characteristic

When impedance relays are designed with a directional element, they operate only for specific conditions. In the R-X plane of measured fault impedances, the characteristic of the distance relay appears as a semicircle. The response of the distance relay to faults closer than a fraction of the line length occurs very quickly. Beyond this range, to differentiate the protective functions of different areas of the system, the fault-clearing process must be accompanied by a certain time delay. The functional characteristics of the different protection areas of the directional impedance relay are shown in Figure 11.

In the mho relay, the characteristics of impedance and directional relays are combined, and a resistive element counteracts the directional component using voltage. The mho relay is inherently directional and can encompass the circle by biasing the current or deflecting the coordinate origin in the R-X characteristic of the relay such that the origin lies outside it. The performance characteristic of the fog relay is shown in Figure 12.

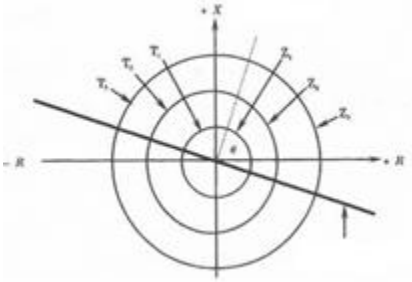

Fig. 11. Functional characteristics of different protection areas of directional impedance relay.

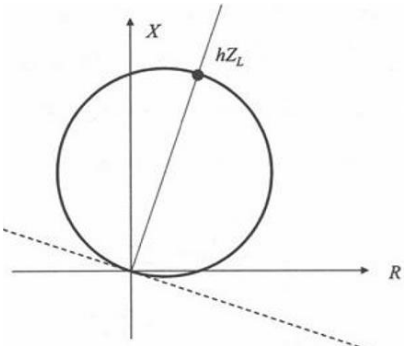

Fig. 12. Performance characteristics of the fog relay

Reactance relays are designed to measure only the reactive component of line impedance. Consequently, their settings are based on reactance. In these types of relays, maximum torque occurs when the current lags the voltage by 90 degrees. In other words, the operating characteristic of the relay is such that all impedance vectors terminating on this characteristic have a constant X component. The characteristic of the reactance relay is shown in Fig. 13.

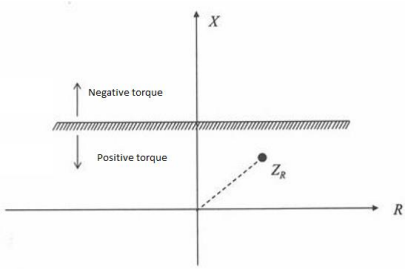

Fig. 13. Characteristic of the reactance relay

Polygonal relays provide a broader range of coverage for fault resistance, especially for short lines, as the position of line resistance can be set in the trip characteristic. The polygonal operating characteristic is derived from three separate measuring elements: reactance, resistance, and directionality. To achieve this characteristic, these measuring elements are suitably combined. The relay issues a trip command only when all three elements operate, thereby achieving the desired polygonal characteristic. The characteristics of polygonal relays are shown in Figure 14.

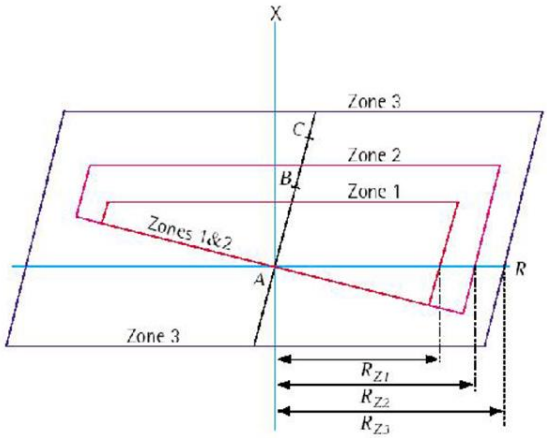

Fig. 14. Characteristics of polygonal relays

The wavelet transform represents a logical next step, employing a windowing method with variable-sized regions. Wavelet transforms allow for longer time intervals when more precise low-frequency information is needed, and shorter intervals when high-frequency information is of interest. Herein lies an issue that seems contrary to time-based, frequency-based, and STFT signal representations:

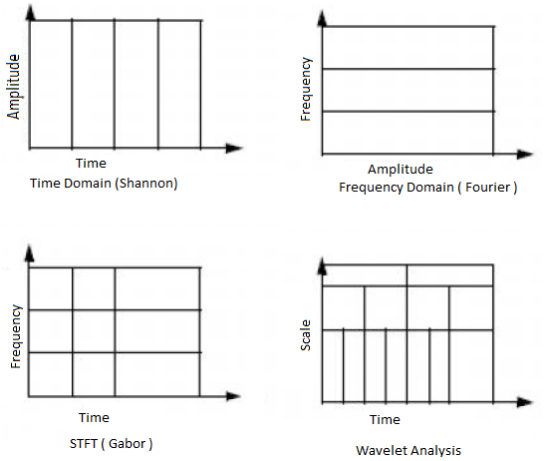

Fig. 15. Windowing method in Fourier transform and wavelet transform

As shown in Figure 15, wavelet transforms utilize time-scale regions instead of time-frequency regions. in One of the major advantages offered by wavelets is their ability to perform localized analyses, meaning analyzing a specific part of a larger signal. According to Figure 16, consider a sinusoidal signal with a small discontinuity, so small that it is hardly visible, such a signal can easily be produced in the real world with power fluctuations or a noisy switch.

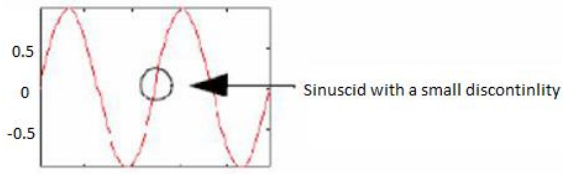

Fig. 16. A sinusoidal signal with small changes

The Fourier coefficient diagram of this signal (plotted using MATLAB's Fourier transform command) is shown in Figure 17 and does not reveal anything particularly interesting; it displays a flat and uniform spectrum with two peaks indicating a specific frequency. However, the wavelet coefficient diagram clearly shows the precise timing location of the discontinuity. Wavelet analysis can reveal aspects of data that other signal analysis methods miss, such as breakdown points, discontinuities in higher derivatives, and self-similarity. Because it can provide different representations of data compared to traditional methods, wavelet analysis can often compress or denoise signals without significant degradation.

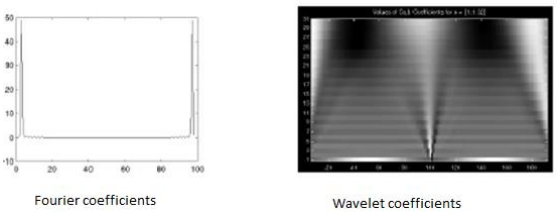

Fig. 17. Fourier coefficient diagram of the sample signal

3. Solution Method

The simulation in this scheme has been carried out in two separate parts, in the protection and operation sections. The simulations were performed using a CPU core i5. In order to evaluate the accuracy of the protective algorithm, a 14-bus IEEE standard power system model was designed for various fault simulations using EMTDC/PSCAD software, as shown in Figure 2. MATLAB software was also used for software programming in both sections. The single-line diagram of the network under study is shown. The table shows the basic information related to the protection section. Figure 18 shows the single-line diagram of the investigated network. Table 1 shows the parameters of the simulated transmission system.

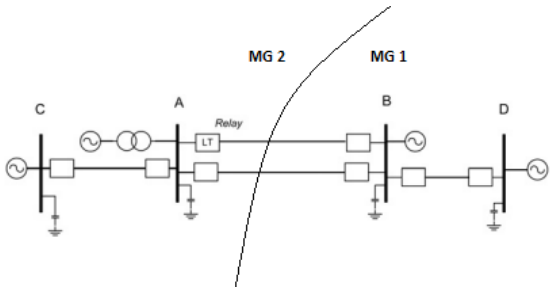

Fig. 18. Single-line diagram

Table.1.
The parameters of the simulated transmission system

Source A: $z_1 = 0.81 + j9.45, z_0 = 1.6 + j9.34\ \Omega$
Nominal voltage = 230 kV
Source B: $z_1 = 0.61 + j9.15, z_0 = 0.75 + j9.15\ \Omega$
Nominal voltage = 400 kV
Source C: $z_1 = 1.9 + j19, z_0 = 2.38 + j19.1\ \Omega$
Nominal voltage = 400 kV
Source D: $z_1 = 2.3 + j23, z_0 = 2.86 + j22.9\ \Omega$
Nominal voltage = 400 kV
Transformer A: 230/400k, 700 MVA
Transmission lines: $z_1 = 0.0264 + j0.3,\ z_0 = 0.275 + j1.08\ \Omega$
ABL 160 km, AC: 270 km, BD: 90km
Bus equivalent capacitance = 0.02 μF

4. Protection Section Simulation:

The appropriate mother wavelet for extracting transient signals should be capable of providing high amplitude and low oscillation output in response to the difference between received signals. To select the appropriate mother wavelet, numerous simulations were performed based on the selected features and the introduced wavelets in the MATLAB software toolbox on a 14-bus IEEE standard network, ultimately selecting the 1 db mother wavelet as the most suitable one. Considering the frequency band of transient waves caused by faults in transmission lines, a signal sampling frequency of 200 kHz was chosen. A wide range of simulation studies was conducted for various types of faults, including single-phase to

ground fault, double-phase to ground fault, double-phase fault, three-phase fault, transient conditions, network configuration changes, line disconnection and reconnection, transformers, capacitor banks, and reactors. For example, one case of internal fault and one case of external microgrid fault were modeled. The proposed protective algorithm is shown in the figure 19. Fault identification methods are also shown in the figures. In the figure 19 the maximum modal current signals at a frequency of 50-100 kHz are used in determining the circuit under fault. If this is $\frac{|I\alpha_1|}{|I\alpha_2|} > Th_2\ OR\ \frac{|I\beta_1|}{|I\beta_2|} > Th_2\ OR\ \frac{|I\gamma_1|}{|I\gamma_2|} > Th_2$, the fault has occurred in circuit 1. If this is is $\frac{|I\alpha_2|}{|I\alpha_1|} > Th_2\ OR\ \frac{|I\beta_2|}{|I\beta_1|} > Th_2\ OR\ \frac{|I\gamma_2|}{|I\gamma_1|} > Th_2$, the fault has occurred in circuit 2, and if this is is $\frac{|I\alpha_1|}{|I\alpha_2|} \approx Th_2\ AND\ \frac{|I\beta_1|}{|I\beta_2|} \approx Th_2\ AND\ \frac{|I\gamma_1|}{|I\gamma_2|} \approx Th_2$, an external fault has occurred. That $|I\alpha_1|, |I\alpha_2|, |I\beta_1|, |I\beta_2|, |I\gamma_1|, |I\gamma_2|$ is, the maximum magnitude of the traveling waves is the modal components of parallel lines. The Th_2 threshold is for detecting and distinguishing between internal and external errors. Figure 20. Flowchart of the proposed fault-type (Ground faults) classification algorithm. First, the current signal is measured using the zero sequence component. Faults are divided into two categories: ground and non-ground. If the zero-sequence current is greater than a specified threshold, a ground fault can be inferred. If none of the criteria defined for single-phase faults are met, the algorithm starts to determine the faulted phases in a multi-phase fault. Figure 21. Flowchart of the proposed fault-type (Ground faults) classification algorithm. When a phase-to-phase fault occurs, the reflected traveling waves in the faulted phases have the same amplitude but opposite signs. This feature is used to detect non-earth faults. Figure 22. Proposed algorithm for the classification of non-ground inter-circuit faults. Figure 25 The flowchart shows the problem solving. This flowchart is related to sections 2 and 3. Which proceeds after the error occurs. Unnecessary loads are removed and multiple scenarios are examined and using cooperative game theory we will have the best choice for energy balance and MOP index.

Table 2 presents some results for internal and external faults under different fault conditions for faults on circuits 1 between buses MG1 and MG2. It should be noted that since both circuits are parallel between buses MG1 and MG2, simulation results for faults on circuit 1 only are presented here. In all studied cases, the protective algorithm is capable of distinguishing and classifying faults correctly and quickly. The conversion of modal β and γ fault current signals in phase C and the current signals of both parallel circuits are shown in Figure 23.

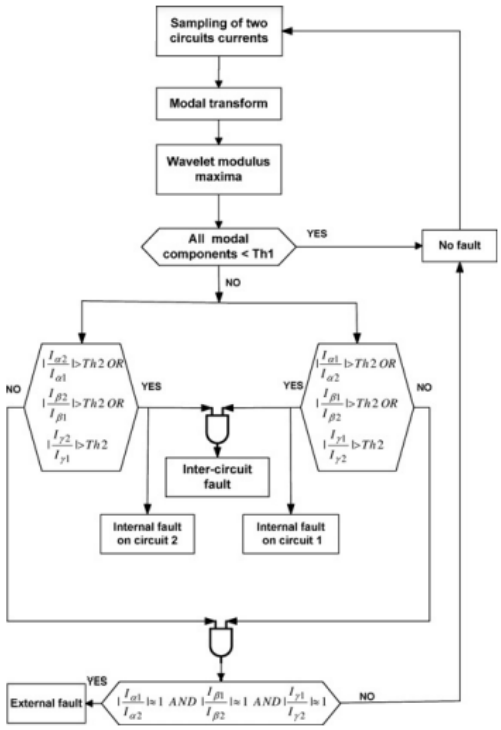

Fig. 19. Proposed protection flowchart

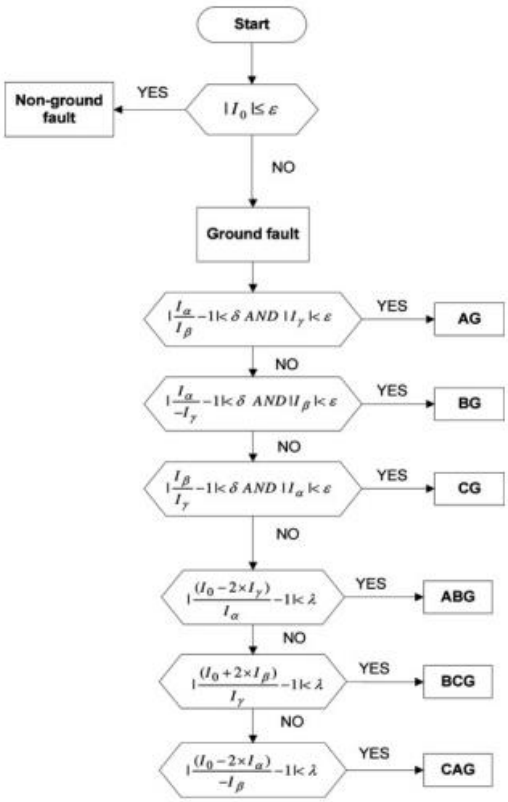

Fig. 20. Flowchart of the proposed fault-type (Ground faults) classification algorithm

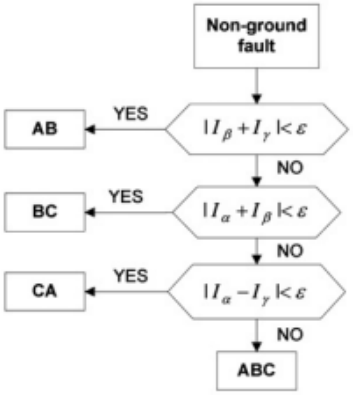

Fig. 21. Flowchart of the proposed fault-type (Ground faults) classification algorithm.

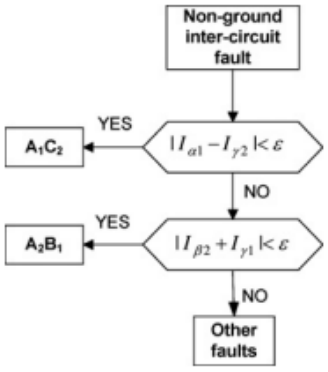

Fig. 22. Proposed algorithm for the classification of non-ground inter-circuit faults

Fig. 23.

A) Internal Fault

For example, in the third column of Table 2, the results obtained for a single-phase internal fault to ground (CG) in MG1 from the protected parallel lines are shown, where the fault occurs 30 kilometers from the relay bus. The calculated ratios for $\frac{I_{\beta 1}}{I_{\beta 2}}, \frac{I_{\gamma 1}}{I_{\gamma 2}}$ are found to be 3.0426 and 3.0446, which exceed the threshold of 2.9413. This indicates that an internal fault has occurred in MG1. The zero-sequence current in MG1 is equal to 0.1007, which is greater than the defined threshold value of 0.01. Therefore, the fault is classified as a ground fault. Since $I_{\alpha 1}$ is zero and the ratio $\frac{I_{\beta 1}}{I_{\gamma 1}}$ is approximately equal to 1, the algorithm classifies the type of fault as a CG fault.

Table.2.
Obtained results for different internal faults

Fault type	*AG*	*CG*	*AB*	*AC*	*ABG*	*BCG*	*ABC*	*AB,BG*
Dis, km	100	30	120	90	120	150	100	50,100
$R_f\Omega$	0.01	0.01	10	10	10	0.01	0.01	5,5
φ	90	10	30	45	30	10	90	60,45
$I_{\alpha 1}$	-1	-0.01	-1.73	-0.30	-1.69	-1.05	-1.91	-0.56
$I_{\beta 1}$	-1.01	0.59	-0.86	-0.6	-0.69	0.87	-2.03	-0.42
$I_{\gamma 1}$	-0.01	0.6	0.88	-0.3	0.99	1.92	-0.12	-.40
I_{o1}	-0.58	-0.66	0	0	0.22	0.1	0	0.25
$I_{\alpha 1}/I_{\alpha 2}$	-2.49	1	-2.67	-2.54	-2.67	-2.98	-2.54	-3.56
$I_{\beta 1}/I_{\beta 2}$	-2.55	-1.93	-2.57	-2.57	-2.58	-2.68	-2.46	-2.63
$I_{\gamma 1}/I_{\gamma 2}$	1	-2.02	-2.78	-2.6	-2.74	-2.84	-1.68	-2.53

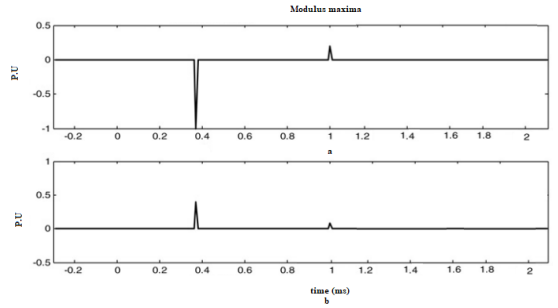

Fig. 24. WTMM of α-modal currents for an internal AG fault. a: For circuit 1 (faulted circuit) b: For circuit 2 (healthy circuit)

B) External fault

Some of the results obtained for external faults under different conditions are presented in Table 3. In this table, the distance of a fault being positive indicates an external fault, while a negative value signifies a fault occurring in the reverse direction. The modal α , β transformation of current signals in phases B and C to ground in Figure 24 is shown. For example, in the fourth column of Table 3, the results obtained for an external fault at a distance of 30 kilometers show a calculated ratio $\frac{I_{\alpha 1}}{I_{\alpha 2}}, \frac{I_{\beta 1}}{I_{\beta 2}}, \frac{I_{\gamma 1}}{I_{\gamma 2}}$ of 1, indicating that the disturbance identified is an external fault in the protected parallel transmission lines. It should be noted that due to the desired margin between characteristic values for internal and external faults, even if the parallel lines are not identical, the proposed criterion is capable of identifying external faults effectively. In this table, for external faults, a positive distance value indicates a forward fault, while a negative value signifies a fault occurring in the reverse direction.

Table.3.
Obtained result for different external faults

Fault type	*Identical circuits*				*Non- identical circuits*			
Dis, km	*AG*	*BG*	*CG*	*BCG*	*AG*	*BC*	*BCG*	*ABCG*
$R_f\Omega$	5	60	30	0	5	60	30	0
φ	0.01	0.01	0	10	0.01	0.01	10	10
$I_{\alpha 1}$	10	60	90	270	10	60	90	270
$I_{\beta 1}$	-0.028	0.239	0.185	0.287	-0.03	0.244	0.185	-0.295
$I_{\gamma 1}$	-0.030	0.221	0.264	-0.290	-0.031	-0.239	0.255	-0.286
$I_{\alpha 1}/I_{\alpha 2}$	-0.003	0.460	0.081	0.012	-0.003	-0.455	0.08	0.01
$I_{\beta 1}/I_{\beta 2}$	1	1	1	1	1.09	1.09	1.1	1.08
$I_{\gamma 1}/I_{\gamma 2}$	1	1	1	1	1.08	1.09	1.11	1.09

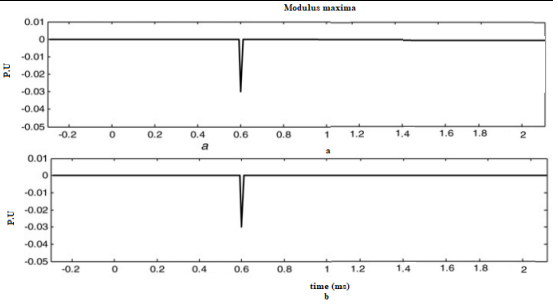

Fig. 25. WTMM of α-modal currents for an external AG fault on the remote transmission line BD a: For circuit 1 b: For circuit 2

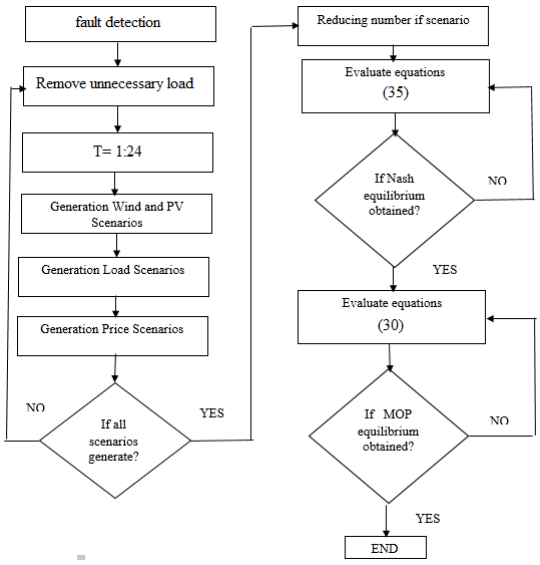

Fig. 26. Problem solving flowchart

Figure 26. It shows the responsive loads for each micro grid, Figure 27 shows the load balance for micro grid 1. For example, at hour 1, micro grid 1 has 30 kW more energy than the load. who has sold this extra amount. Also, the participating elements in energy production for 1 hour are DG, CHP and wind turbine. Figure 28, shows the load balance for micro grid 1. For example, in hour 1, micro grid 2 has purchased 30 kW of electrical energy. It has produced 10 kW of wind energy, 15 kW of DG and 5 kW of CHP. Figure 29 shows the electrical energy balance among micro grids. According to Figure 29, it can be seen that in hours 1, 2, and 24, micro grid 1 has sold electrical energy to micro grid 2. In hours 16, micro grid 2 has sold electric power to micro grid 1. In some hours, the request to buy and sell was without result, which shows that buying in these hours was not suitable considering the price. These results were obtained using the cooperative game model in game theory and the players (micro grids) reaching Nash equilibrium. Figure 30 examines the self-healing subscribers in two cases. The network collapsed in the first case, regardless of resilience, after the occurrence of a connection and a lack of compensation, but it was able to survive again in the second case, which was accompanied by timely identification and fast compensation.

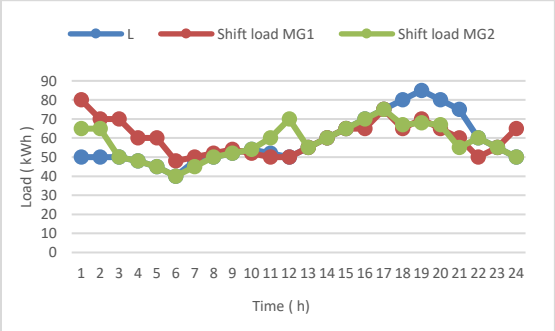

Fig. 27. Responsive load

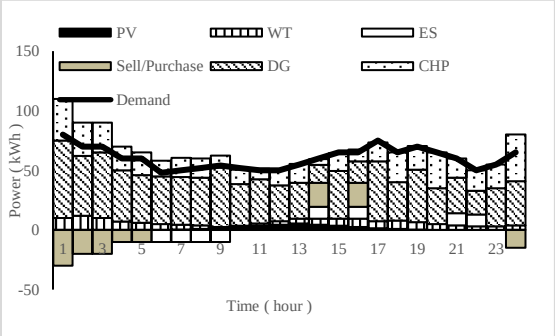

Fig. 28. Load balancing MG1

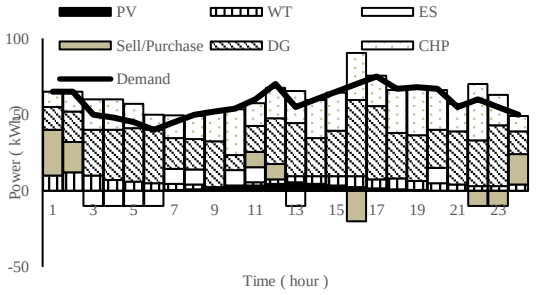

Fig. 29. Load balancing MG2

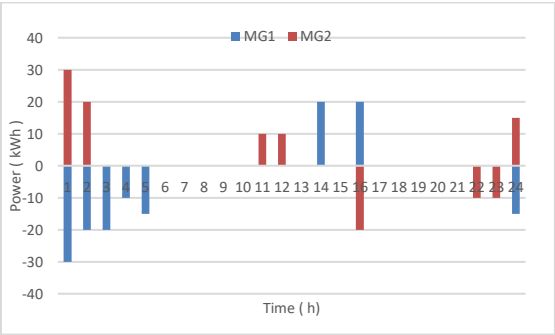

Fig. 30. The electrical energy balance among micro grids.

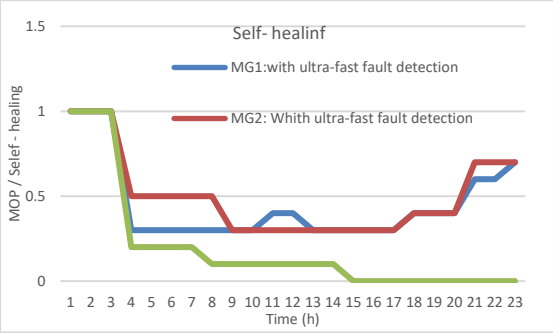

Fig. 31. Self- Healing index

5. Conclusion

Having a resilient distribution network is one of the most essential needs of a power system when facing short-circuit faults. In the first stage, the essential need is the rapid identification and elimination of faults. The aim of this scheme is to improve the resilience and operation of two microgrids in islanded mode using a fast algorithm to identify various types of faults within and outside the microgrids. At this stage, the proposed algorithm works as follows: protection algorithm based on the primary current traveling waves it is caused by errors that are detected by relays using wavelet conversion. In mode Internal errors on each of the parallel lines, traveling waves of current detected in phases corresponding parallel lines are different, while for external errors these waves are approximately are similar .This feature is used to distinguish between internal and external errors. Also, the algorithm for classifying the type of error is checked to identify the phases under error. This algorithm can also cover inter-circuit faults in which phases of both parallel circuits are involved in the fault. The protection algorithm can detect internal and external faults and also identify the faulted phases with high reliability. After fault identification, compensation for faults is provided using D-STATCOM. The operation process is based on CPP pricing in a way that the microgrids strive to maintain resilience and prevent each other from blackouts by exchanging surplus power. In summary, the results can be categorized as follows:

- Rapid identification of various types of short-circuit faults within and outside microgrids
- Fault compensation using D-STATCOM
- Improvement of resilience in critical conditions
- Enhancement of self-healing (MOP)

Therefore, it can be concluded that the proposed plan, i.e. fast fault detection in island microgrids, can prevent the collapse of the network by accurate and fast fault detection as well as timely compensation. Also, by improving reliability and improving resilience, the MOP index is also improved.

References

[1] Lachovicz, Felipe J., Thelma SP Fernandes, and João A. Vilela Junior. "Impacts of PV-STATCOM Reactive Power Dispatch in the Allocation of Capacitors Bank and Voltage Regulators on Active Distribution Networks." Journal of Control, Automation and Electrical Systems (2023): 1-12.

[2] Sousa, Renata Oliveira de, et al. "Modulation Strategy Impact on the Energy Storage Requirements of Modular Multilevel Converter-Based STATCOM." Journal of Control, Automation and Electrical Systems (2023): 1-11.

[3] Babaei, Mohammad Amin, Saeed Hasanzadeh, and Hamid Karimi. "Cooperative energy scheduling of interconnected microgrid system considering renewable energy resources and electric vehicles." Electric Power Systems Research 229 (2024): 110167.

[4] Azimian, Mahdi, et al. "Resilience-oriented planning of multi-carrier microgrids under cyber-attacks." Sustainable Cities and Society 79 (2022): 103709.

[5] Коцур, Михаил, et al. "Accuracy improvement for the determination of parameters and voltage drops in busbars, considering the networks power factor." Problemele energeticii regionale 51.3 (2021): 37-52.

[6] Rahmatian, Mohammad Rasoul, Ahmad Ghaderi Shamim, and Salah Bahramara. "Optimal operation of the energy hubs in the islanded multi-carrier energy system using Cournot model." Applied Thermal Engineering 191 (2021): 116837.

[7] Azizi, Ali Akbar, Ahmad Ghaderi Shamim, and Mohamad Ehsan Mosayebian. "Robust island-mode operation of power distribution network using game theory for resilience enhancement." Sustainable Energy, Grids and Networks 33 (2023): 100978.

[8] Amini, Fariba, et al. "A stochastic two-stage microgrid formation strategy for enhancing distribution network resilience against earthquake event incorporating distributed energy resources, parking lots and responsive loads." Sustainable Cities and Society 101 (2024): 105191.

[9] Tejaswini, V., and D. Susitra. "Optimal Location and Compensation Using D-STATCOM: A Hybrid Hunting Algorithm." Journal of Control, Automation and Electrical Systems 32.4 (2021): 1002-1023.

[10] Thongsuk, Surakit, et al. "An approach for voltage drop improvement in 22 kV PEA distribution system based on high voltage capacitor placement." Energy Reports 9 (2023): 48-54.

[11] Mumtaz, Faisal, et al. "Ultra high-speed fault diagnosis scheme for DC distribution systems based on discrete median filter and mathematical morphology." IEEE Access 12 (2024): 45796-45810.